RSC Advances

PAPER

Cite this: *RSC Adv.*, 2020, **10**, 36828

Novel porous iron phthalocyanine based metal–organic framework electrochemical sensor for sensitive vanillin detection†

Jinyun Peng, *[a] Liying Wei,[ab] Yuxia Liu,[c] Wenfeng Zhuge,[a] Qing Huang,[a] Wei Huang,[a] Gang Xiang[a] and Cuizhong Zhang[a]

Received 6th August 2020
Accepted 22nd September 2020

DOI: 10.1039/d0ra06783k

rsc.li/rsc-advances

Vanillin is widely used as a flavor enhancer and is known to have numerous other interesting properties, including antidepressant, anticancer, anti-inflammatory, and antioxidant effects. However, as excess vanillin consumption can affect liver and kidney function, simple and rapid detection methods for vanillin are required. Herein, a novel electrochemical sensor for the sensitive determination of vanillin was fabricated using an iron phthalocyanine (FePc)-based metal–organic framework (MOF). Scanning electron microscopy and transmission electron microscopy showed that the FePc MOF has a hollow porous structure and a large surface area, which impart this material with high adsorption performance. A glassy carbon electrode modified with the FePc MOF exhibited good electrocatalytic performance for the detection of vanillin. In particular, this vanillin sensor had a wide linear range of 0.22–29.14 μM with a low detection limit of 0.05 μM (S/N = 3). Moreover, the proposed sensor was successfully applied to the determination of vanillin in real samples such as vanillin tablets and human serum.

1. Introduction

Vanillin (4-hydroxy-3-methoxybenzaldehyde), the major component of *Vanilla planifolia*, a large orchid plant, is mainly derived from vanilla beans or pods.[1] Due to the unique aromatic properties, vanillin is one of the most commonly produced spices globally, and it is widely used as a flavor enhancer for candy, ice cream, wine, and other food products.[2] In addition, vanillin has been found to have antidepressant, anticancer, anti-inflammatory, and antioxidant effects, and shows potential as a food preservative.[3–6] However, excessive vanillin intake can affect liver and kidney function, causing symptoms such as headaches, nausea, and vomiting.[7] Therefore, it is necessary to develop simple and rapid detection methods for vanillin.

Various analytical methods have been developed for the determination of vanillin, including gas chromatography–mass spectrometry, high-performance liquid chromatography, thin-layer chromatography, capillary electrophoresis, and UV-Vis spectrometry.[8–12] Despite the good selectivity and high accuracy of these methods, they are time-consuming and costly, and most require complicated sample pretreatment before analysis. In recent years, electrochemical (EC) methods have attracted extensive attention because of their high sensitivity, high selectivity, low cost, fast response, and operational simplicity. As vanillin has electrochemically active groups, it can be detected electrochemically. However, there are few studies on the electrochemical detection of vanillin, mainly because the overpotential for vanillin oxidation on a bare electrode is too high and the easy adsorption of the oxidation products on the electrode surface causes electrode poisoning.[13] These issues could be overcome *via* electrode modification. Therefore, it is important to develop new chemically modified electrodes for the sensitive detection of vanillin.

Metal–organic frameworks (MOFs) are porous crystalline materials with periodic network structures formed by metal ions/clusters and organic ligands connected through coordination bonds.[14–16] MOFs, which have the advantages of large specific surface areas, high porosities, and adjustable pore sizes, have been widely studied in fields such as energy storage, gas storage and separation, catalysis, and sensors.[16–20] The advantageous characteristics of MOFs combined with the simplicity, low cost, and high sensitivity of electrochemical sensors has made the development of MOF-based electrochemical sensors of particular recent interest.[21–24]

Phthalocyanine, one of the most investigated functional organic materials, has a two-dimensional conjugated macrocyclic structure with 18π electrons that is composed of four isoindole rings connected by nitrogen atoms.[25–27] The

[a]College of Chemistry and Chemical Engineering, Guangxi Normal University for Nationalities, Chongzuo 532200, China. E-mail: pengjinyun@yeah.net; Fax: +86 771 7870799; Tel: +86 771 7870653

[b]School of Pharmacy, Henan University of Traditional Chinese Medicine, Zhengzhou 450046, China

[c]College of Physics and Electronic Engineering, Guangxi Normal University for Nationalities, Chongzuo 532200, China

† Electronic supplementary information (ESI) available. See DOI: 10.1039/d0ra06783k

phthalocyanine structure is similar to the porphyrin structure, but phthalocyanine is easier to synthesize. In addition, the application range of phthalocyanine exceeds that of porphyrin owing to the enhanced stability, spectral characteristics, coordination characteristics, and structural flexibility of phthalocyanine.[28] Phthalocyanine can coordinate different metals to form metal phthalocyanine (MPc) complexes, which have unique electronic and optical properties, including good electron-transfer performance and redox activity.[28–31] In addition, phthalocyanine derivatives, in which hydrogen on the phthalocyanine benzene rings is substituted with functional groups such as amino carboxyl, or nitro groups, can exhibit increased reactivity for MPc formation and expand the application field.[32–34] Owing to their unique structures and various functional properties, including excellent semiconductor properties and catalytic activities, MPc derivatives have been widely used in various fields including catalysis, sensors, and photodynamic therapy.[35–42] Due to its redox activity, catalytic activity, and carrier transport ability result from the extended π-system, MPc complexes have been used as the linking units in 2D MOFs, which show good stability, conductivity, redox activity, and electrocatalytic activity.[43–45]

Here, we developed a novel electrochemical sensor based on an iron phthalocyanine (FePc) MOF for the sensitive detection of vanillin. The electrochemical behavior of vanillin on a glassy carbon electrode (GCE) modified with the FePc MOF was systematically investigated, and the developed sensor was applied to the detection of vanillin in real samples such as vanillin tablets and human serum. To the best of our knowledge, this is the first example of an electrochemical sensor based on a phthalocyanine derived MOF.

2. Experimental

2.1 Reagents and apparatus

Trimellitic anhydride, urea, anhydrous $FeCl_3$, ammonium molybdate, trifluoroacetic acid (TFA), iron(III) nitrate nonahydrate ($Fe(NO_3)_3 \cdot 9H_2O$), sodium acetate trihydrate ($NaOOCCH_3 \cdot 3H_2O$), and *N*,*N*-dimethylformamide (DMF) were purchased from Aladdin Reagent Co., Ltd. (Shanghai, China). Britton–Robinson (B–R) buffer solutions (0.1 M) with different pH values were prepared by mixing stock solutions of 0.04 M H_3PO_4, H_3BO_3, CH_3COOH, and 0.2 M NaOH. All reagents were of analytical grade and used directly without further purification. Double distilled water was used in all experiments.

All electrochemical measurements were performed on a CHI 760E electrochemical workstation (Shanghai Chenhua Instrument Co., Ltd., Shanghai, China) using a GCE working electrode, Pt counter electrode, and Ag/AgCl reference electrode. The FePc MOF material was characterized using scanning electron microscopy (SEM, Hitachi S-4800, Tokyo, Japan; 15 kV), transmission electron microscopy (TEM, JEM 2100, JEOL, Japan; 200 kV), Fourier transform infrared (FT-IR) spectroscopy (Spectrum 65, PerkinElmer, Waltham, USA), X-ray diffraction (XRD, D8 advance, Bruker, Germany) and X-ray photoelectron spectroscopy (XPS, K-Alpha, Thermo Scientific, USA).

2.2 Synthesis of materials

2.2.1 Synthesis of tetracarboxylic iron phthalocyanine (TCFePc). TCFePc was synthesized using a previously reported method with some improvements.[30] Typically, trimellitic anhydride (33 g), urea (60 g), anhydrous $FeCl_3$ (7.80 g), and ammonium molybdenate (0.50 g) were ground and mixed thoroughly. The mixture was reacted at 140 °C for 1 h and then at 190 °C for 4 h. Subsequently, boiling water was added to the product. After filtration, the precipitate was washed with boiling water and methanol, and then dried under vacuum at 50 °C for 24 h to give tetraformamido iron phthalocyanine. This product was mixed with 1 M hydrochloric acid in a saturated sodium chloride solution (500 mL) and boiled for 3 min. After cooling, suction filtration was performed and the filter cake was transferred to a round-bottom flask. After adding 2 M sodium hydroxide in a saturated sodium chloride solution (500 mL), the mixture was refluxed at 90 °C for 12 h. The product was diluted 5 times water and subjected to suction filtration. The pH of the filtrate was adjusted to <3 by adding concentrated hydrochloric acid. After standing overnight, the precipitate was collected by suction filtration, washed with boiling water, methanol, and ether, and finally dried under vacuum to obtain TCFePc.

2.2.2 Synthesis of $[Fe_3O(OOCCH_3)_6OH] \cdot 2H_2O$. $[Fe_3O(OOCCH_3)_6OH] \cdot 2H_2O$ was synthesized by dissolving $Fe(NO_3)_3 \cdot 9H_2O$ (8 g) and $Na(OOCCH_3) \cdot 3H_2O$ (11 g) in 9 mL of deionized water and allowing the obtained solution to stir overnight at room temperature. A red precipitate was obtained by filtration, washed once with cold deionized water, and dried in an oven at 100 °C. Finally, the crystalline product was obtained by recrystallization from DMF.

2.2.3 Synthesis of FePc MOF. The FePc MOF material was synthesized using a solvothermal method.[46] $[Fe_3O(OOCCH_3)_6OH] \cdot 2H_2O$ (80 mg) and TCFePc (80 mg) were ultrasonically dissolved in 16 mL of DMF, and then 2.4 mL of TFA was added. The resulting solution was placed in a 50 mL Teflon-lined stainless steel reaction kettle and heated at 150 °C for 12 h. After cooling to room temperature, the reaction mixture was centrifuged at 7000 rpm for 5 min, washed 3 times with acetone, and then dried under vacuum to obtain the FePc MOF.

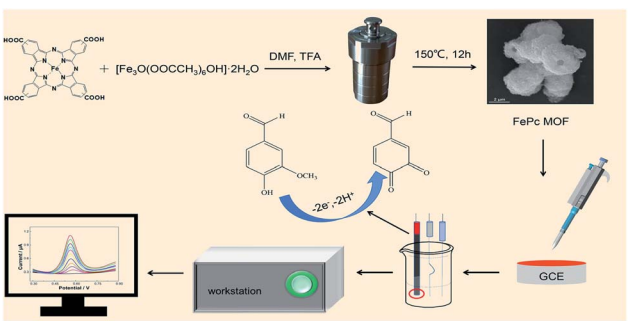

Scheme 1 Fabrication of FePc MOF/GCE modified electrode and electrochemical determination of vanillin.

2.3 Preparation of modified electrode

Prior to modification, the GCE was polished with 0.3 and 0.05 μm alumina slurries to remove adsorbed organic substances and then washed by sonication in ethanol and double distilled water. The FePc MOF (1.5 mg) was dispersed in 1 mL of DMF under sonication for 40 min. Next, 3 μL of 1.5 mg mL^{-1} FePc MOF suspension was dropped onto the surface of GCE and dried under infrared light to prepare FePc MOF/GCE. Scheme 1 illustrates the Fabrication of FePc MOF/GCE modified electrode and electrochemical determination of vanillin.

2.4 Preparation of samples

Vanillin tablets were obtained from China Pharmaceutical University Pharmaceutical Co., Ltd. (0.2 g × 36 tablets). Twenty tablets were ground into a fine powder. Then, a precisely weighed amount of powder (~0.2 g vanillin) was dissolved in ethanol. After filtering the solution, 5 mL of the filtrate was diluted 50 times with ethanol. The human serum samples, which were collected from Chongzuo People's Hospital (Guangxi, China), were mixed with anhydrous ethanol at 1 : 3 (v/v) and centrifuged at 10 000 rpm for 10 min.

3. Results and discussion

3.1 Characterization of FePc-based MOF

The surface morphology of the FePc MOF was characterized using SEM and TEM (Fig. 1). The SEM image (Fig. 1A) indicates that the FePc MOF material has a hollow porous structure, which was further confirmed by the hollow structure (Fig. 1B) and pore structure (Fig. 1C) observed in the TEM images. Fig. 1D shows the FT-IR spectra of FePc and the FePc MOF. For FePc (Fig. 1D, red), the peak at 1698 cm^{-1} corresponds to the telescopic vibration absorption peak of C=O, whereas the peaks at 1333, 1147, 1086, 857, and 739 cm^{-1} are assigned to the characteristic absorption peaks of the phthalocyanine macroring. Similar peaks are observed for the FePc MOF (Fig. 1D, black) but the intensities are reduced.

XPS was used to analyze the chemical composition of FePc MOF, and the results showed the presence of C, N, O, Fe, and F elements in the sample (Fig. S1A†). In the Fe 2p spectrum (Fig. S1B†), two sets of peaks at 710.9 and 724.8 eV, assignable to Fe $2p_{3/2}$ and Fe $2p_{1/2}$, respectively, revealing the oxidation state of +3 for Fe in the FePc MOF.[47] Moreover, the two satellite peaks at 718.8 and 733.1 eV, which further proves the existence of Fe^{3+}. Fig. S1D† shows The XRD pattern of FePc MOF (black curve). The diffraction peaks are consistent with the simulation results (red curve).

3.2 Electrochemical behavior of FePc MOF

3.2.1 Electrochemical impedance spectroscopy (EIS). EIS can be used to study the resistance of different electrodes. Nyquist plots in the frequency range from 0.1 to 10^5 Hz were obtained for a bare GCE and the FePc MOF/GCE in a 1.0 mM $[Fe(CN)_6]^{3-/4-}$ solution (Fig. 2A). The Nyquist plots consist of two main regions, namely, a linear region at lower frequencies and a semicircular region at higher frequencies, which represent the diffusion process and the charge-transfer resistance (R_{ct}), respectively.[48] As shown in Fig. 2A, in the frequency range of 1 to 10^5 Hz, the R_{ct} of the bare GCE is ~950 ohm. The diameter of the semicircle in the Nyquist plot is significantly larger for the bare GCE than for the modified electrode, which indicates that the bare GCE has a smaller surface area and lower

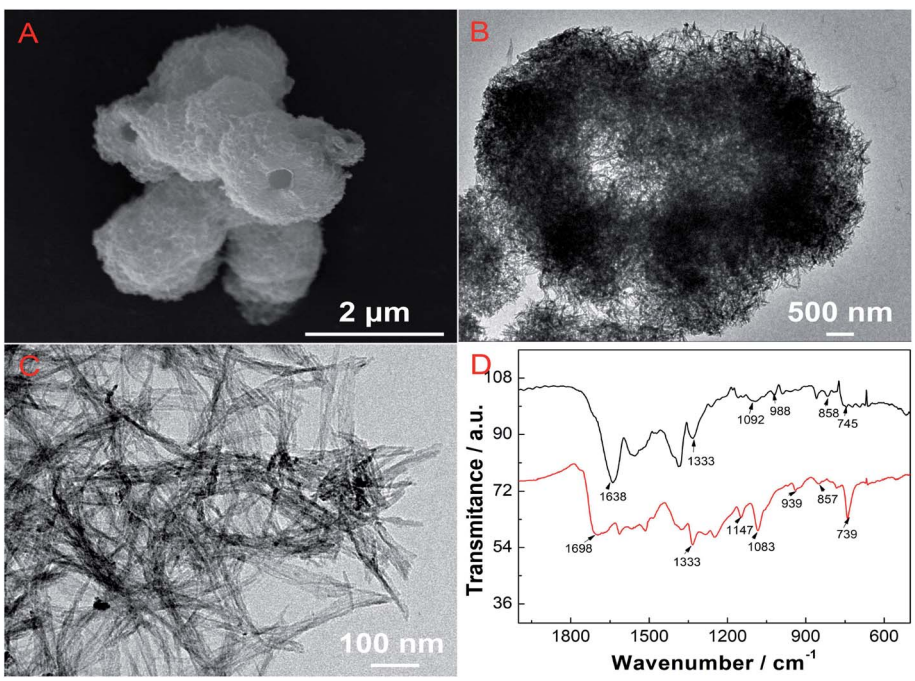

Fig. 1 (A) SEM and (B and C) TEM images of FePc MOF. (D) FT-IR spectra of FePc (red) and FePc MOF (black).

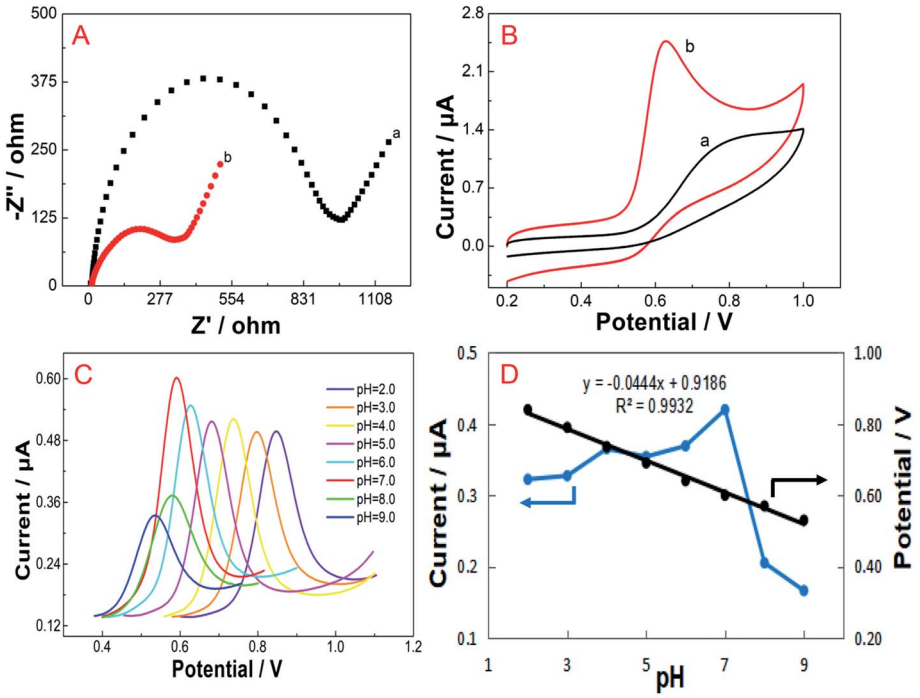

Fig. 2 (A) Nyquist plots for bare GCE (a) and FePc MOF/GCE (b) in 1.0 mM $[Fe(CN)_6]^{3-/4-}$ ($K_3Fe(CN)_6/K_4Fe(CN)_6 = 1:1$, containing 0.1 M KCl). (B) Cyclic voltammograms of 65.46 μM vanillin on bare GCE (a) and FePc MOF/GCE (b) in B–R buffer (pH 7.0). Scan rate = 0.1 V s^{-1}. (C) Differential pulse voltammograms of 15 μM vanillin in 0.1 M B–R buffer at different pH values (2.0–9.0) obtained using the FePc MOF/GCE and (D) changes in the oxidation peak current and potential as a function of pH.

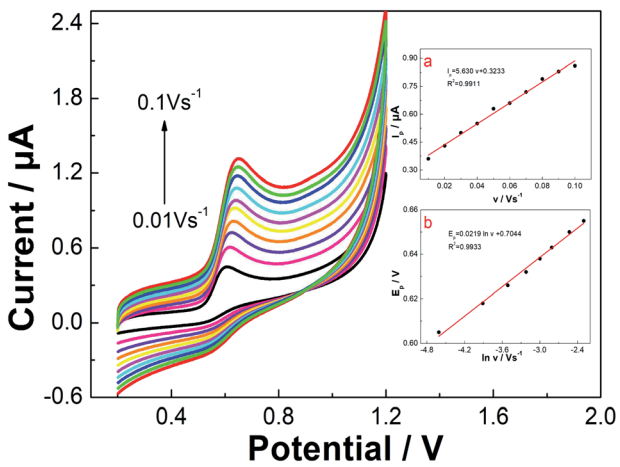

Fig. 3 Cyclic voltammograms of FePc MOF/GCE in 0.1 M B–R buffer (pH 7.0) containing 15 μM vanillin collected at different scan rates (0.01–0.1 V s^{-1}). Inset a: linear relationship between the oxidation current (I_p) and the scan rate (v). Inset b: linear relationship between the oxidation peak potential (E_p) and the natural logarithm of the scan rate (ln v).

electron conductivity. The lower R_{ct} of the FePc MOF/GCE (~328 ohm) suggests that the redox reaction of $[Fe(CN)_6]^{3-/4-}$ is significantly accelerated on the surface of the modified electrode. This result clearly demonstrates that the introduction of the FePc MOF material onto the GCE surface can reduce the electron-transfer resistance.

3.2.2 Enhanced oxidation of vanillin at FePc MOF/GCE. The electrochemical behavior of vanillin at the bare GCE and FePc MOF/GCE was studied using cyclic voltammetry (CV) in B–R buffer (pH 7.0) containing 65.46 μM vanillin. Within the potential window of 0.2–1.0 V, a weak oxidation peak is observed with the bare GCE (Fig. 2B). However, with the FePc MOF/GCE, a significant oxidation peak is observed at ~0.62 V, indicating the good electron-transfer performance of the FePc MOF. Moreover, Fig. S2† shows the CV of without and with vanillin on FePc MOF/GCE. It can be seen that FePc MOF/GCE has no oxidation peak in blank buffer solution, indicating that the FePc MOF/GCE can be used to determine vanillin. A comparison of the oxidation peak currents of vanillin on the bare GCE and FePc MOF/GCE reveals that the FePc MOF imparts enhanced sensitivity and catalyzes the electro-oxidation of vanillin on the GCE. We attribute the high peak current of FePc MOF/GCE to its porous structure, as vanillin can pass through these pores and reach the electrode surface more easily.

3.3 Effect of pH

The electrochemical responses of vanillin on the FePc MOF/GCE in B–R buffer solutions at pH 2.0–9.0 were studied using differential pulse voltammetry (DPV), as shown in Fig. 2C. The oxidation peak current of vanillin increases slowly from pH 2.0 to 6.0, reaches a maximum value at pH 7.0, and then gradually decreases from pH 7.0 to 9.0. Therefore, pH 7.0 B–R buffer was selected for vanillin analysis. In addition, as the pH value increases from 2.0 to 9.0, the

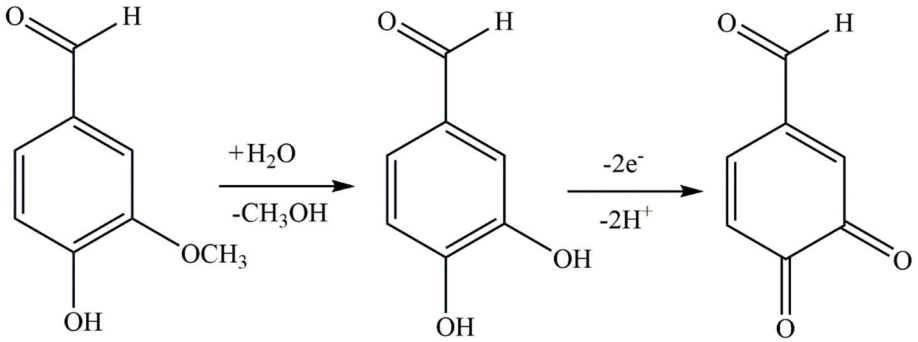

Scheme 2 Proposed mechanism for the oxidation of vanillin at FePc MOF/GCE.

oxidation peak potential (E_p, V) obviously decreases, indicating that protons participate in the oxidation reaction. A linear relationship was observed between E_p and pH, as described by the equation $E_p = 0.9186 - 0.0444$ pH ($R^2 = 0.9932$) (Fig. 2D). The slope of -44.4 mV pH^{-1} demonstrated that the numbers of transferred protons and electrons are the same during the electrochemical oxidation of vanillin.

3.4 Effect of scan rate

Determining the influence of the scan rate on electrochemical behavior is an effective method for exploring the mechanism of an electrode surface reaction. The effect of the scan rate on the electrochemical performance of the FePc MOF/GCE for the oxidation of vanillin was investigated using CV (Fig. 3). In B–R buffer (pH 7.0), the oxidation peak current (I_p) of vanillin exhibits a good linear relationship with the scan rate (v) in the range of 0.01–0.1 V s^{-1}, as described by the equation $I_p = 0.3233 + 5.630v$ ($R^2 = 0.9911$). This result indicates that the oxidation of vanillin on the surface of the FePc MOF/GCE is a typical adsorption-controlled process.

In addition, the oxidation peak potential (E_p) is shifted positively as the scan rate increased, which indicates that the oxidation process is irreversible. The linear relationship between the oxidation peak potential and the natural logarithm of the scan rate (ln v) can be expressed as $E_p = 0.0219(\ln v) + 0.7044$ ($R^2 = 0.9933$). For an irreversible and adsorption-controlled oxidation process, the correlation between the E_p and ln v can be described using Laviron's theory:[49]

$$E_p = E^{0\prime} + \frac{RT}{\alpha nF}\ln\frac{RTk^0}{\alpha nF} + \frac{RT}{\alpha nF}\ln v$$

here, $E^{0\prime}$ is the formal standard potential, R is the gas constant, T is the absolute temperature, α is the charge transfer coefficient, n is the number of transferred electrons, k^0 is the standard rate constant of the reaction, v is the scanning rate, and F is the Faraday constant. Using this equation, αn can be calculated as 1.17. As α is generally assumed to be 0.5 for an irreversible electrochemical

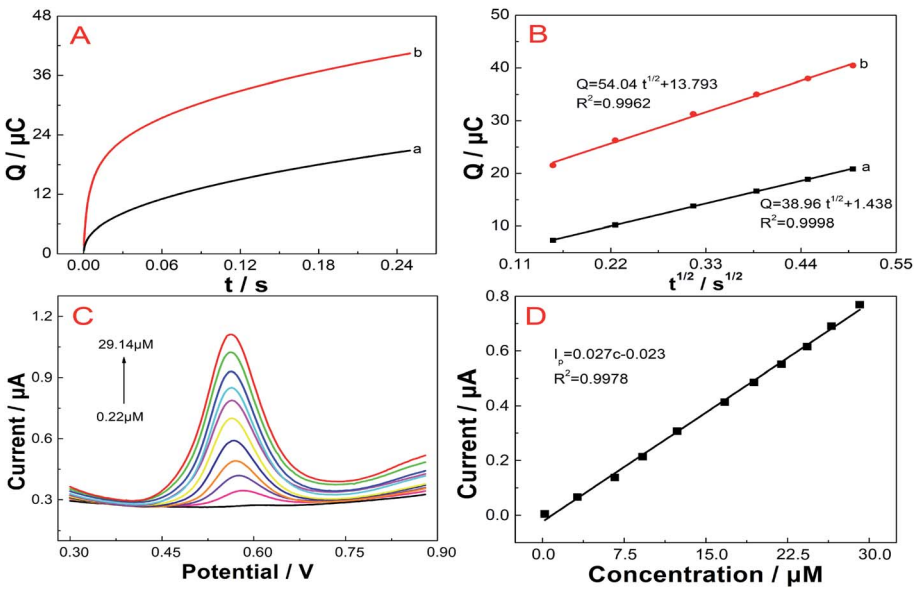

Fig. 4 (A) Q–t curves of bare GCE (a) and FePc MOF/GCE (b). (B) Linearized Q–$t^{1/2}$ plots for bare GCE (a) and FePc MOF/GCE (b). (C) Differential pulse voltammograms of FePc MOF/GCE in 0.1 M B–R buffer with 0.22–29.14 μM vanillin. (D) Linear relationship between the oxidation peak current and the vanillin concentration.

Table 1 Comparison of different electrochemical electrodes for vanillin determination

Electrode	Technique	Linear range (μmol L^{-1})	LOD (μmol L^{-1})	Reference
Au–Ag alloy NP[a]/GCE	Amperometry[j]	0.2–50	0.04	53
BDD[b]	SWV[k]	3.3–98	0.16	55
Arg-G[c]/GCE	DPV	2–70	1	56
Al–TiO_2-NPs/SPCE[d]	LSV[l]	0.07–20	0.02	57
MWNTs-PDA@MIP/SWNTs-COOH[e]/GCE	DPV	0.2–10	0.1	58
Aptamer-AuNPs/FcKB/ZIF-8[f]@GCE	SWV	0.01–200	0.03	59
MoS_2–CNF[g]/GCE	*I–T*[m]	0.3–135	0.15	60
CTABMGPE[h]	DPV	4–15 and 20–70	1.29	61
CoS NR@nafion-GCE	DPV	0.5–56	0.07	62
G-QD[i]@Nafion/AuNPSPCE	LSV and DPV	13–660 and 0.66–33	3.9 and 0.32	63
FePc MOF/GCE	DPV	0.22–29.14	0.05	This work

[a] Nanoparticles. [b] Boron-doped diamond electrode. [c] Arginine-functionalized graphene. [d] Screen-printed carbon electrode. [e] Polydopamine-functionalized multi-walled carbon nanotubes, MIP and carboxyl single-walled carbon nanotubes composite. [f] Ketjen black/ferrocene dual-doped zeolite-like MOFs and electrodeposited gold nanoparticles coupled with DNA aptamer. [g] Carbon nanofibers. [h] CTAB-modified graphene paste electrode. [i] Graphene-quantum dots. [j] Amperometry: amperometric measurements. [k] Square wave voltammetry. [l] Linear sweep voltammetry. [m] Current–time.

reaction, the value of n is approximately 2. Furthermore, from the relationship between E_p and pH, the numbers of transferred protons and electrons are the same. Therefore, it can be concluded that the oxidation process of vanillin at FePc MOF/GCE involves two protons and two electrons, which is consistent with previously reported results.[50–52] The proposed mechanism for vanillin oxidation is shown in Scheme 2.

3.5 Chronocoulometry analysis

The effective surface areas of the bare GCE and FePc MOF/GCE were analyzed by chronocoulometry. Fig. 4A shows the Q–t curves of the bare GCE and FePc MOF/GCE in 1 mM $K_3Fe(CN)_6$ containing 0.1 M KCl. Fig. 4B shows the linearized Q–$t^{1/2}$ plots, where gave equations of Q (μC) = $38.96t^{1/2}$ + 1.438 (R^2 = 0.9998) and Q (μC) = $54.04t^{1/2}$ + 13.739 (R^2 = 0.9962) for bare GCE and FePc MOF/GCE, respectively. The slopes of the Q–$t^{1/2}$ plots can be expressed as $2nFAcD^{1/2}/\pi^{1/2}$, as in the Anson equation:[53]

$$Q = \frac{2nFAcD^{1/2}t^{1/2}}{\pi^{1/2}} + Q_{dl} + Q_{ads}$$

where A (cm^2) is the surface area of the electrode; c is the vanillin concentration; D is the apparent diffusion coefficient; F is the Faraday constant; n is the number of electrons transferred, Q_{dl} (C) is the double-layer charge, which can be eliminated by background subtraction; and Q_{ads} (C) is Faradaic charge due to the oxidation of adsorbed vanillin. For 1 mM $K_3Fe(CN)_6$, n can be considered equal to 1 and D equal to 7.6×10^{-6} cm^2 s^{-1}.[54] Thus, using the slopes of the linear plots, the A values for bare GCE and FePc MOF/GCE were calculated as 0.129 and 0.180 cm^2, respectively. These results indicate that modification with FePc MOF increases the specific surface area of the electrode, thus providing more reaction sites and improving the detection sensitivity.

3.6 Vanillin detection

Under the optimal conditions, the electrochemical response of FePc MOF/GCE to vanillin at different concentrations was studied using DPV. As shown in Fig. 4C and D, the peak current increases with increasing vanillin concentrations, and a good linear relationship ($I_p = 0.027c - 0.023$, $R^2 = 0.9978$) is observed between the vanillin concentration and its oxidation peak current in the range of 0.22–29.14 μM. The limit of detection (LOD, S/N = 3) was calculated as 0.05 μM.

The proposed method was compared with previous reported electrochemical methods for vanillin detection (Table 1). It can be seen that the FePc MOF/GCE provides a reasonable linear range for vanillin detection and has a lower LOD, which is comparable to other sensors.

3.7 Reproducibility, stability, and interference

To evaluate the reproducibility of the sensor, the DPV current responses to 1.5 μM vanillin were used. Eleven consecutive measurements with the same electrode gave a relative standard deviation (RSD) for the response peak current of 2.02%. Measurements with five independently prepared electrodes gave an RSD of 1.25%. These results indicate that the sensor has good reproducibility. To evaluate stability, the modified electrode was stored at 4 °C for 1 week. After week, the sensor maintained 93% of the initial peak current, indicating good storage stability.

Table 2 Effects of interfering substances on the sensor to vanillin

Interferent	n^a	Er (%)	Interferent	n^a	Er (%)
Glucose	300	−1.49	Na^+	100	−0.82
Sucrose	300	0.70	Mg^{2+}	50	−3.92
Maltose	100	−1.96	Zn^{2+}	50	2.17
Starch	50	−2.27	Cu^{2+}	50	2.27
Dextrin	50	−3.80	Fe^{3+}	500	−0.03
Glycine	50	−2.12	Al^{3+}	500	2.33
L-Leucine	100	1.40	NH_4^+	50	−1.55
L-Gystein	50	0.45	SO_4^{2-}	500	−0.03
L-Phenylalanine	50	−2.34	Cl^-	100	−0.82
Ascorbic acid	10	4.92	HCO_3^-	100	−3.92
K^+	200	−2.30	CO_3^{2-}	50	1.55
Ca^{2+}	100	1.19	NO_3^-	50	0.80

[a] Molar ratio (interfering substances/vanillin).

The selectivity of the sensor was evaluated by examining the interference of possible coexisting substances in drug and biological samples. The results are shown in Table 2, using a 1.5 μM vanillin standard solution, no interference (deviation <5%) with 500-fold Fe^{3+}, Al^{3+}, and SO_4^{2-}; 300-fold glucose and sucrose; 200-fold K^+; 100-fold maltose, L-leucine, Ca^{2+}, Na^+, HCO_3^-, and Cl^-; 50-fold starch, dextrin, L-gystein, L-phenylalanine, Mg^{2+}, Zn^{2+}, Cu^{2+}, NH_4^+, CO_3^{2-}, NO_3^-; and 10-fold ascorbic acid. Fig. S3† showed the DPV of 1.5 μM vanillin at FePc MOF/GCE when coexisting with 150 μM UA and DA. It can be seen that owing to the oxidation potential differences, the oxidation peak of vanillin (oxidation peak: 0.5–0.70 V) is significantly higher than UA (oxidation peak: 0.2–0.5 V) and less than DA (oxidation peaks: 0.9–1.1 V). Therefore, the interference of UA and DA can be ignored when the interference analysis ratio is 100 : 1. These results indicate that the FePc MOF/GCE had good selectivity for vanillin determination.

3.8 Analysis of real samples

To evaluate the practicality of the developed sensor, the feasibility of vanillin detection in vanillin tablets and human serum was investigated using DPV under the optimized conditions. As shown in Table S1,† satisfactory vanillin recoveries were obtained using the FePc MOF/GCE. Moreover, the vanillin contents determined using the FePc MOF/GCE were in good agreement with those obtained by UV analysis, indicating that the sensor has good application potential for determining the vanillin content of real samples (Table S2†).

4. Conclusions

In this work, a novel electrochemical sensor was developed for the determination of vanillin by modifying a GCE with FePc MOF. The good electrocatalytic performance of the FePc MOF may be due to its pore structure, which can absorb vanillin and accelerate the electron-transfer rate, thus increasing the oxidation rate. The fabricated sensor exhibited a linear response range for vanillin of 0.22–29.14 μM with an LOD of 0.05 μM. Moreover, the prepared sensor was successfully applied to detect the content of vanillin in tablets and human serum.

Conflicts of interest

There are no conflicts to declare.

Acknowledgements

This work was supported by the Natural Science Foundation of Guangxi Province [grant no. 2016GXNSFAA380113, 2018JJA12000] and the National Natural Science Foundation of China [grant no. 21465004].

References

1 F. Shakee, N. Haq, N. A. Siddiqui, F. K. Alanazi and I. A. Alsarra, *Food Chem.*, 2015, **188**, 57–61.
2 Z. Dong, F. Gu, F. Xu and Q. Wang, *Food Chem.*, 2014, **149**, 54–61.
3 A. Shoeb, M. Chowta, G. Pallempati, A. Rai and A. Singh, *Indian J. Pharmacol.*, 2013, **45**, 141–144.
4 S. Srinual, P. Chanvorachote and V. Pongrakhananon, *Int. J. Oncol.*, 2017, **50**, 1341–1351.
5 M. E. Kim, J. Y. Na, Y. D. Park and J. S. Lee, *Appl. Biochem. Biotechnol.*, 2019, **187**, 884–893.
6 I. Mourtzinos, S. Konteles, N. Kalogeropoulos and V. T. Karathanos, *Food Chem.*, 2009, **114**, 791–797.
7 L. Jiang, Y. Ding, F. Jiang, L. Li and F. Mo, *Anal. Chim. Acta*, 2014, **833**, 22–28.
8 N. Ochiai, K. Sasamoto, A. Hoffmann and K. Okanoya, *J. Chromatogr. A*, 2012, **1240**, 59–68.
9 C. Liu, L. Zhao, Z. Sun, N. Cheng, X. Xue, L. Wu and W. Cao, *Anal. Methods*, 2018, **10**, 743–748.
10 S. S. Hingse, S. B. Digole and U. S. Annapure, *J. Anal. Sci. Technol.*, 2014, **5**, 21.
11 M. Shu, Y. Man, H. Ma, F. Luan, H. Li and Y. Gao, *Food Anal. Methods*, 2016, **9**, 1706–1712.
12 N. Altunay, *LWT–Food Sci. Technol.*, 2018, **93**, 9–15.
13 F. Bettazzi, I. Palchetti, S. Sisalli and M. Mascini, *Anal. Chim. Acta*, 2006, **555**, 134–138.
14 H.-C. Zhou, J. R. Long and O. M. Yaghi, *Chem. Rev.*, 2012, **112**, 673–674.
15 H.-C. Zhou and S. Kitagawa, *Chem. Soc. Rev.*, 2014, **43**, 5415–5418.
16 G. Cai and H.-L. Jiang, *Angew. Chem., Int. Ed.*, 2017, **56**, 563–567.
17 T. Mehtab, G. Yasin, M. Arif, M. Shakeel, R. M. Korai, M. Nadeem, N. Muhammad and X. Lu, *J. Energy Storage*, 2019, **21**, 632–646.
18 H. Li, L. Li, R.-B. Lin, W. Zhou, Z. Zhang, S. Xiang and B. Chen, *EnergyChem*, 2019, **1**, 100006.
19 L. Chen and Q. Xu, *Matter*, 2019, **1**, 57–89.
20 E. Naghian, E. M. Khosrowshahi, E. Sohouli, F. Ahmadi, M. R. Nasrabadi and V. Safarifard, *New J. Chem.*, 2020, **44**, 9271–9277.
21 C. Bao, Q. Niu, Z.-A. Chen, X. Cao, H. Wang and W. Lu, *RSC Adv.*, 2019, **9**, 29474–29481.
22 Z. Zeng, X. Fang, W. Miao, Y. Liu, T. Maiyalagan and S. Mao, *ACS Sens.*, 2019, **4**, 1934–1941.
23 X. Fang, X. Chen, Y. Liu, Q. Li, Z. Zeng, T. Maiyalagan and S. Mao, *ACS Appl. Nano Mater.*, 2019, **2**, 2367–2376.
24 X. Fang, B. Zong and S. Mao, *Nano-Micro Lett.*, 2018, **10**, 64.
25 Z. Liu, Q. Jiang, R. Zhang, R. Gao and J. Zhao, *Electrochim. Acta*, 2016, **187**, 81–91.
26 N. Masilela and T. Nyokong, *Dyes Pigm.*, 2010, **84**, 242–248.
27 A. Gelir, İ. Yılmaz and Y. Yılmaz, *J. Phys. Chem. B*, 2007, **111**, 478–484.
28 M. K. Sener, A. Koca, A. Gül and M. B. Kocak, *Polyhedron*, 2007, **26**, 1070–1076.
29 N. Silva, C. Castro-Castillo, M. P. Oyarzún, S. Ramírez, C. Gutierrez-Ceron, J. F. Marco, J. F. Silva and J. H. Zagal, *Electrochim. Acta*, 2019, **308**, 295–306.
30 M. Arıcı, D. Arıcan, A. L. Uğur, A. Erdoğmuş and A. Koca, *Electrochim. Acta*, 2013, **87**, 554–566.

31 K. Sakamoto and E. Ohno, *Dyes Pigm.*, 1997, **35**, 375–386.
32 J. Peng, Q. Huang, Y. Liu, F. Liu and C. Zhang, *Sens. Actuators, B*, 2019, **294**, 157–165.
33 T. Xu, D. Wang, L. Dong, H. Shen, W. Lu and W. Chen, *Appl. Catal., B*, 2019, **244**, 96–106.
34 D. Yu and X. He, *Appl. Mater. Today*, 2016, **3**, 1–10.
35 J. Peng, W. Zhuge, Y. Liu, C. Zhang, W. Yang and Y. Huang, *J. Electrochem. Soc.*, 2019, **166**, B1612–B1619.
36 Y.-J. Yuan, J.-R. Tu, H.-W. Lu, Z.-T. Yu, X.-X. Fan and Z.-G. Zou, *Dalton Trans.*, 2016, **45**, 1359–1363.
37 C. Li, T. Huang, Z. Huang, J. Sun, C. Zong, J. Yang, W. Deng and F. Dai, *Dalton Trans.*, 2019, **48**, 17258–17265.
38 C. Marinescu, M. B. Ali, A. Hamdi, Y. Cherifi, A. Barras, Y. Coffinier, S. Somacescu, V. Raditoiu, S. Szunerits and R. Boukherroub, *Chem. Eng. J.*, 2018, **336**, 465–475.
39 J. Peng, Q. Huang, W. Zhuge, Y. Liu, C. Zhang, W. Yang and G. Xiang, *Biosens. Bioelectron.*, 2018, **106**, 212–218.
40 J. Peng, W. Zhuge, Y. Huang, C. Zhang and W. Huang, *Bull. Korean Chem. Soc.*, 2019, **40**, 214–219.
41 Y. Baygu and Y. Gök, *Inorg. Chem. Commun.*, 2018, **96**, 133–138.
42 Z. Huang, L. Huang, Y. Huang, Y. He, X. Sun, X. Fu, X. Xu, G. Wei, D. Chen and C. Zhao, *Nanoscale*, 2017, **9**, 15883–15894.
43 H. Nagatomi, N. Yanai, T. Yamada, K. Shiraishi and N. Kimizuka, *Chem. – Eur. J.*, 2018, **24**, 1806–1810.
44 H. Zhong, K. H. Ly, M. Wang, Y. Krupskaya, X. Han, J. Zhang, J. Zhang, V. Kataev, B. Büchner, I. M. Weidinger, S. Kaskel, P. Liu, M. Chen, R. Dong and X. Feng, *Angew. Chem., Int. Ed.*, 2019, **31**, 10677–10682.
45 H. Jia, Y. Yao, J. Zhao, Y. Gao, Z. Luo and P. Du, *J. Mater. Chem. A*, 2018, **6**, 1188–1195.
46 L. Sun, J. Xie, Z. Chen, J. Wu and L. Li, *Dalton Trans.*, 2018, **47**, 9989–9993.
47 T. Yamashita and P. Hayes, *Appl. Surf. Sci.*, 2008, **254**, 2441–2449.
48 W. Cai, T. Lai, H. Du and J. Ye, *Sens. Actuators, B*, 2014, **193**, 492–500.
49 E. Laviron, *J. Electroanal. Chem.*, 1979, **101**, 19–28.
50 T. T. Calam and D. Uzun, *Electroanalysis*, 2019, **31**, 2347–2358.
51 A. T. Ezhil Vilian, P. Puthiaraj, C. H. Kwak, S.-K. Hwang, Y. S. Huh, W.-S. Ahn and Y.-K. Han, *ACS Appl. Mater. Interfaces*, 2016, **8**, 12740–12747.
52 D. Y. Zheng, C. G. Hua, T. Gan, X. P Dang and S. S. Hu, *Sens. Actuators, B*, 2010, **148**, 247–252.
53 F. C. Anson, *Anal. Chem.*, 1964, **36**, 932–934.
54 Y. Wang, Y. Ding, L. Li and P. Hu, *Talanta*, 2018, **178**, 449–457.
55 Y. Yardım, M. Gülcan and Z. Şentürk, *Food Chem.*, 2013, **141**, 1821–1827.
56 Y. Zhao, Y. Du, D. Lu, L. Wang, D. Ma, T. Ju and M. Wu, *Anal. Methods*, 2014, **6**, 1753–1758.
57 K. Murtada, S. Jodeh, M. Zougagh and Á. Ríos, *Electroanalysis*, 2018, **30**, 969–974.
58 W. Wu, L. Yang, F. Zhao and B. Zeng, *Sens. Actuators, B*, 2017, **239**, 481–487.
59 Y. Sun, X. Jiang, H. Jin and R. Gui, *Anal. Chim. Acta*, 2019, **1083**, 101–109.
60 Q. Mei, Y. Ding, L. Li, A. Wang, D. Duan and Y. Zhao, *J. Electroanal. Chem.*, 2019, **833**, 297–303.
61 C. Raril and J. G. Manjunatha, *Microchem. J.*, 2020, **154**, 104575.
62 M. Sivakumar, M. Sakthivel and S.-M. Chen, *J. Colloid Interface Sci.*, 2017, **490**, 719–726.
63 G. M. Durán, E. J. Llorent-Martínez, A. M. Contento and Á. Ríos, *Microchim. Acta*, 2018, **185**, 204.